

Vapour-phase deposition of oriented copper dicarboxylate metal-organic framework thin films

Stassin, Timothée; Rodriguez-Hermida, S.; Schrode, B.; Cruz, Alexander John; Carraro, F.; Kravchenko, D.; Creemers, V.; Stassen, I.; Hauffman, Tom; De Vos, Dirk; Falcaro, P.; Resel, R.; Ameloot, R.

Published in:
Chemical Communications

DOI:
[10.1039/c9cc05161a](https://doi.org/10.1039/c9cc05161a)

Publication date:
2019

License:
Unspecified

Document Version:
Accepted author manuscript

[Link to publication](#)

Citation for published version (APA):

Stassin, T., Rodriguez-Hermida, S., Schrode, B., Cruz, A. J., Carraro, F., Kravchenko, D., Creemers, V., Stassen, I., Hauffman, T., De Vos, D., Falcaro, P., Resel, R., & Ameloot, R. (2019). Vapour-phase deposition of oriented copper dicarboxylate metal-organic framework thin films. *Chemical Communications*, 55(68), 10056-10059. <https://doi.org/10.1039/c9cc05161a>

Copyright

No part of this publication may be reproduced or transmitted in any form, without the prior written permission of the author(s) or other rights holders to whom publication rights have been transferred, unless permitted by a license attached to the publication (a Creative Commons license or other), or unless exceptions to copyright law apply.

Take down policy

If you believe that this document infringes your copyright or other rights, please contact openaccess@vub.be, with details of the nature of the infringement. We will investigate the claim and if justified, we will take the appropriate steps.

ChemComm

Chemical Communications

Accepted Manuscript

This article can be cited before page numbers have been issued, to do this please use: T. Stassin, S. Rodriguez-Hemida, B. Schrode, A. J. Cruz, F. Carraro, D. Kravchenko, V. Creemers, I. Stassen, T. Hauffman, D. E. De Vos, P. Falcato, R. Resel and R. Ameloot, *Chem. Commun.*, 2019, DOI: 10.1039/C9CC05161A.



This is an Accepted Manuscript, which has been through the Royal Society of Chemistry peer review process and has been accepted for publication.

Accepted Manuscripts are published online shortly after acceptance, before technical editing, formatting and proof reading. Using this free service, authors can make their results available to the community, in citable form, before we publish the edited article. We will replace this Accepted Manuscript with the edited and formatted Advance Article as soon as it is available.

You can find more information about Accepted Manuscripts in the [Information for Authors](#).

Please note that technical editing may introduce minor changes to the text and/or graphics, which may alter content. The journal's standard [Terms & Conditions](#) and the [Ethical guidelines](#) still apply. In no event shall the Royal Society of Chemistry be held responsible for any errors or omissions in this Accepted Manuscript or any consequences arising from the use of any information it contains.

COMMUNICATION

Vapour-phase deposition of oriented copper dicarboxylate metal-organic framework thin films

Received 00th January 20xx,
Accepted 00th January 20xx

DOI: 10.1039/x0xx00000x

Copper dicarboxylate metal-organic framework films are deposited via chemical vapour deposition. Uniform films of CuBDC and CuCDC with an out-of-plane orientation and accessible porosity are obtained from the reaction of Cu and CuO with vaporised dicarboxylic acid linkers.

Metal-organic frameworks (MOFs) are microporous crystalline materials built from metal ion nodes connected by multitopic organic linkers. Because of their record-breaking specific surface area (up to $> 7500 \text{ m}^2 \text{ g}^{-1}$) and functionalisable pore interior, MOFs have been extensively studied.^{1–3} Interestingly, the same properties that make MOFs high-performance materials for adsorptive separations also promise high potential in microelectronics.^{4–6} However, the integration of MOFs in microelectronic devices is rarely reported due to a lack of methods to deposit and pattern MOF thin films in a way that is compatible with current microfabrication protocols.⁴ MOFs are typically obtained through solvothermal treatment of an organic linker and metal salt dissolved in an organic solvent.¹ Besides the environmental impact related to the use of solvents, the deposition of MOF films *via* wet protocols can lead to contamination and corrosion issues, for instance due to the presence of salts and particle formation.⁷

Alternative routes for the synthesis of MOF powders make use of non-salt metal precursors (e.g., metal oxides) and little to no solvent. In particular, thermochemical (by heating the linker and precursor together),^{8,9} mechanochemical (neat, ion-, or liquid-assisted grinding)^{10–13} and accelerated aging processes^{14,15} have been proven successful.¹⁶ Contact with bulk

solvent can also be avoided by reacting a drop-casted synthesis solution containing metal salt and organic linker in a saturated solvent atmosphere, yielding highly oriented MOF films.¹⁷

Inspired by the vapour-phase deposition methods common in microfabrication, similar approaches were developed to grow MOF films. Stassen *et al.* introduced the concept of MOF chemical vapour deposition (MOF-CVD), in which a metal oxide precursor layer is first deposited and subsequently transformed to a MOF upon reaction with linker vapour.¹⁸ Directly reacting the surface in an alternating fashion with vaporised metal and linker precursors, has also been reported. This strategy resulted in non-porous, yet crystalline coordination compounds and amorphous layers that yield MOFs after a post-deposition crystallization step.^{19–21}

Here we report the CVD of MOFs based on Cu(II) and the dicarboxylate linkers 1,4-benzendicarboxylic acid (H_2BDC) and *trans*-1,4-cyclohexanedicarboxylic acid (H_2CDC). The resulting CuBDC and CuCDC materials consist of 4-connected Cu(II) carboxylate chains that line one-dimensional pores of 5.3 and 3.5 Å in diameter[†], respectively.^{22,23} The MOF-CVD method for these materials consists of two steps: (i) vapour-phase deposition of Cu or CuO films as a metal source and (ii) a solid-vapour reaction between this precursor and the vaporised organic linker (**Figure 1**). Interestingly, the CuBDC and CuCDC MOF thin films grow with an out-of-plane orientation, with the pores normal to the surface.

CuCDC and CuBDC films were obtained on silicon or glass substrates (ESI Figures S6 and S8[†]). CuO and Cu precursor layers were deposited *via* physical vapour deposition (PVD), an established method available in any microfabrication facility. The surface of metallic Cu is terminated by a CuO layer. Thermal

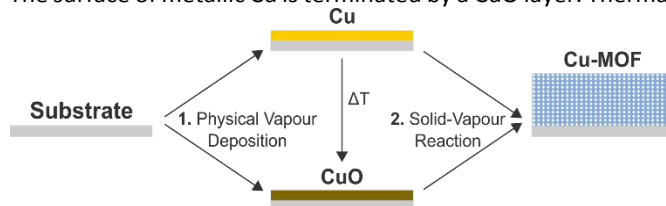


Figure 1 Chemical vapour deposition of Cu-based MOF thin films (MOF-CVD), a two-step process: CuO or Cu precursor layer deposition and subsequent solid-vapour reaction of this layer with dicarboxylic acid linker vapour.

^a Centre for Membrane Separations, Adsorption, Catalysis and Spectroscopy for Sustainable Solutions (cMACS), KU Leuven, Celestijnenlaan 200F box 2454, 3000 Leuven, Belgium.

^b Institute of Solid State Physics, Graz University of Technology, Petersgasse 16, 8010 Graz, Austria.

^c Department of Materials and Chemistry, Research group Electrochemical and Surface Engineering, Vrije Universiteit Brussel, Pleinlaan 2, 1050 Brussels, Belgium.

^d Institute of Physical and Theoretical Chemistry, Graz University of Technology, Stremayrgasse 9/22, 8010 Graz, Austria.

[†] Electronic Supplementary Information (ESI) available: acknowledgments, materials and methods, Cu(II) precursor characterisation (ellipsometry, XRR, XPS), optical images, GIXRD patterns, SEM images, AFM investigation, film thickness by ellipsometry, thermogravimetric analysis, ATR-FTIR data and dihedral angles. See DOI: 10.1039/x0xx00000x

treatment, before or during linker exposure, will result in further oxidation (ESI Figure S3 and Table S4†).²⁴ CuO films of different thicknesses (~ 15 nm and ~ 100 nm) were placed together with excess H₂BDC or H₂CDC in a Schlenk tube and evacuated ($\sim 10^{-1}$ mbar). To study the effect of relative humidity, water was added for a set of experiments to reach a relative humidity of 5% at the reaction temperature. The reaction was performed at 200 °C for 16 hours, followed by thermal activation. Solvent-free activation by thermal treatment has been demonstrated before in the MOF literature, with several examples of dicarboxylic acid linkers thermally desorbed from the MOF pores (e.g., H₂BDC, fumaric acid).^{25–27}

The crystallinity and phase of the resulting films were investigated by synchrotron grazing-incidence X-ray diffraction (GIXRD). The GIXRD data analysed using GIDVis²⁸ was compared with patterns calculated for known crystal structures[†]. Under all conditions phase-pure materials are obtained (Figure 2). Reaction with H₂CDC results in the known porous CuCDC MOF[†] under both dry and humidified conditions. Reaction with H₂BDC under dry conditions yields a phase that strongly resembles the isostructural CuBDC material[†], but with a slight peak shift to higher q values, i.e., a lower interplanar spacing. Reaction with H₂BDC under humidified conditions results in a dense phase that strongly resembles the coordination polymer [Cu₂(OH)₂(BDC)] consisting of Cu(II) hydroxide layers connected by BDC[†],²⁹ but again, peaks are shifted to higher q values. This material is further referred to as CP-CuBDC.

The MOF/CP formation was corroborated by ATR-FTIR spectroscopy (ESI Figure S13 and Table S7†). The absence of a band around 1670 cm⁻¹ indicates that no uncoordinated carboxylic acid is present. The vibrational bands at ~ 1590 cm⁻¹ and ~ 1420 cm⁻¹ are respectively attributed to the asymmetric and symmetric vibrations of metal-coordinated carboxylate groups. All films grown from thin CuO films have a homogeneous, mirror-like appearance and a colour ranging from deep blue to brown (Figure 3, ESI Figure S4†). AFM images show homogeneous films with R_{RMS} roughness values in the 10–30 nm range (Table S6†).

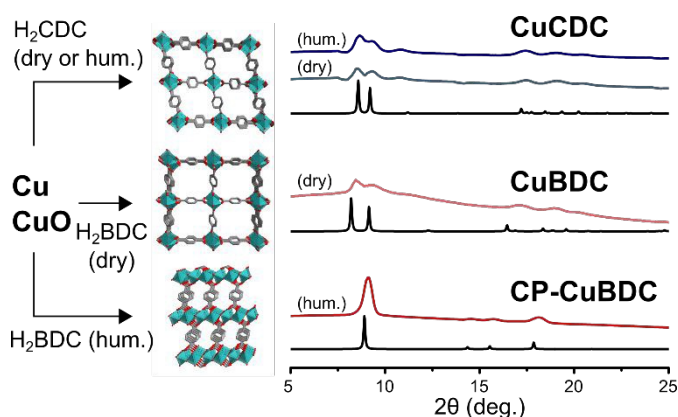


Figure 2 The reactive atmosphere composition (linker and relative humidity) determines the formed MOF structure. Reaction of CuO and Cu with H₂CDC vapour under dry and humidified conditions results in the CuCDC structure. Reaction with H₂BDC under dry conditions results in the CuBDC structure while humidified conditions yield the CP-CuBDC structure. Intensity distribution as a function of 2θ extracted from GIXRD patterns (coloured) and simulated patterns (black).

The total film thickness was determined by ellipsometry and cross-checked by high-resolution cross-sectional SEM, with less than 10% difference between both methods. The thickness for films grown from ~ 15 nm CuO is 50 ± 3 nm for CP-CuBDC, 83 ± 5 nm for CuBDC, 87 ± 5 nm for CuCDC (dry) and 110 ± 8 nm for CuCDC (hum.) (ESI Figure S10†). The thickness of the CuCDC, CuBDC and CP-CuBDC films is lower than expected based on the ratio of the density measured for the CuO film (6.5 g cm^{-3} ; ESI Figure S2 and Table S3†) and calculated for the final materials based on their crystal structure[†]. For this precursor thickness, complete oxide-to-MOF conversion would result in ~ 80 nm CP-CuBDC, ~ 190 nm CuCDC and ~ 200 nm CuBDC films, i.e., an expansion factor of 5, 13 and 13, respectively. Although cross-sectional SEM does not show residual CuO, a few nm of unreacted precursor cannot be ruled out due to the instrument resolution. (Figure 3). When starting from thicker (~ 100 nm) CuO, similar images reveal a ~ 110 nm CuCDC film on top of ~ 90 nm unreacted CuO (Figure 3). These results suggest that only about the first 10 nm of CuO is converted to MOF (ESI Figure S11†), leaving the remaining precursor unreacted. Similar self-limiting MOF growth has previously been observed for ZIF-8 CVD starting from ZnO layers.¹⁸ Although the linkers have a different volatility (higher for H₂CDC) and acidity (higher for H₂BDC), these differences cancel out and result in the same fraction of CuO converted (ESI Figure S12†).

GIXRD indicates that all CuCDC films, independently of the precursor, are oriented with the (100) plane parallel to the

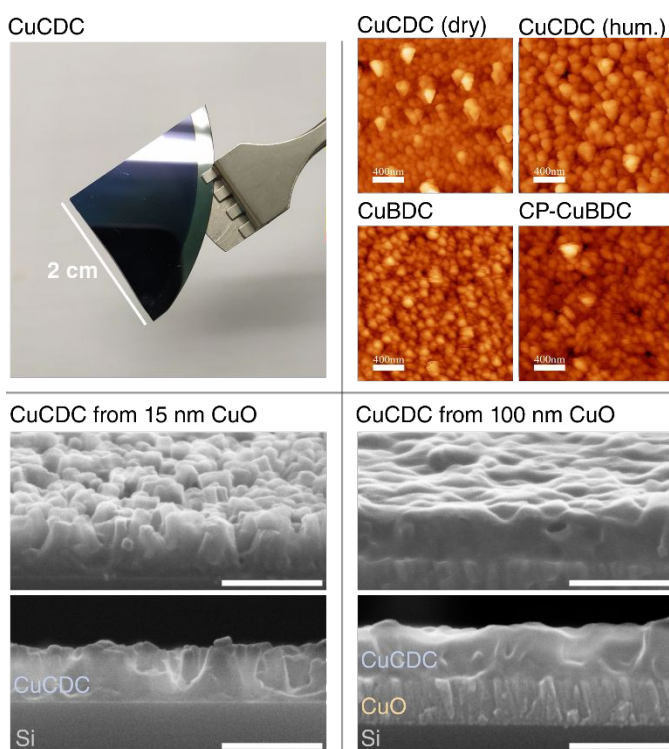


Figure 3 Thin film morphology. Top left: homogeneous, mirror-like CuCDC film. Top right: AFM images of CuCDC films deposited under dry and humidified conditions, and of CuBDC and CP-CuBDC films. Bottom: tilted-view and cross-sectional SEM images of CuCDC film grown from 15 nm of CuO with no residual CuO visible (left) and from 100 nm of CuO layer showing incomplete CuO conversion (right). AFM and SEM scale bars are 400 and 200 nm, respectively. AFM colour scale: see ESI Figure S9†.

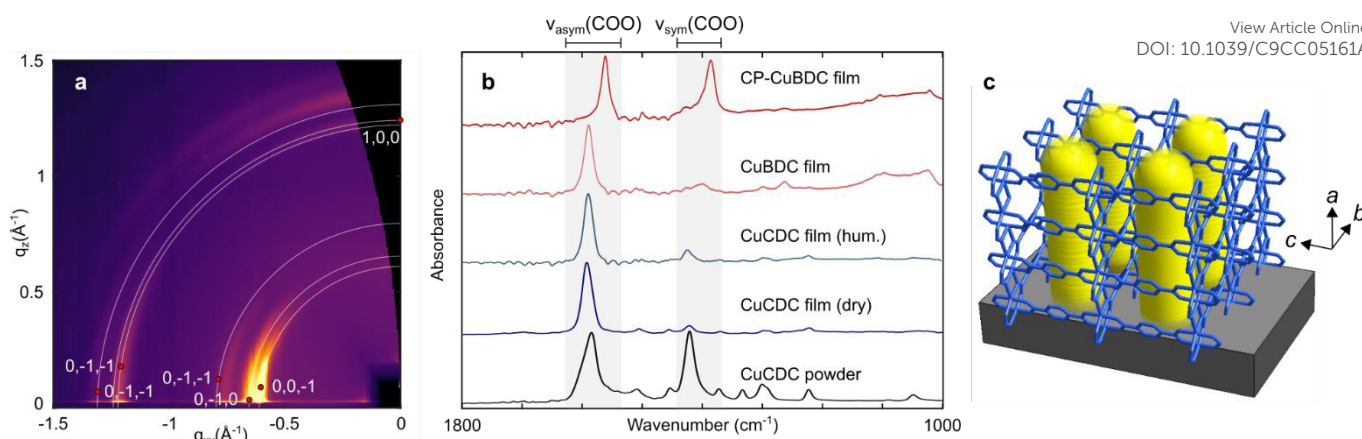


Figure 4 Out-of-plane orientation of CuCDC and CuBDC films. a, GIXRD pattern for CuCDC (dry) overlaid with the Debye-Scherrer diffraction rings (grey lines) and Bragg peak position (red dots) calculated for a (100) orientation. b, Normalised ATR-FTIR spectra of MOF-CVD thin films and bulk CuCDC powder synthesized solvothermally. The carboxylate bands are highlighted in grey. The differences in absorbance between the asymmetric and symmetric vibrations are indicative of the orientation of the carboxylate groups with respect to the substrate. c, Schematic representation of (100)-oriented CuCDC and the resulting pore orientation perpendicular to the substrate highlighted in yellow.

substrate (**Figure 4**, ESI Figure S5[†]). For H₂BDC, the results are different: while the CuBDC MOF is also clearly (100)-oriented, CP-CuBDC shows a weaker and different preferred orientation that depends on the precursor. For CP-CuBDC films prepared from thermal CuO and PVD CuO, the 010 peak at $q \approx 0.64 \text{ \AA}^{-1}$ is found at approximately 20 degrees tilted from the vertical axis. For CP-CuBDC grown from PVD Cu, this off-specular tilt is even stronger. These results indicate a different contact plane than (100) and potentially the presence of multiple orientations (ESI Figure S7[†]).

The (100) orientation of CuBDC and CuCDC films is confirmed by ATR-FTIR using p-polarised light since the absorbance of the asymmetric carboxylate vibration ($\sim 1590 \text{ cm}^{-1}$) is strongly enhanced compared to the symmetric one ($\sim 1410 \text{ cm}^{-1}$) (**Figure 4**). The IR selection rules predict that vibrations normal to the surface give a reduced signal, whereas the signal from vibrations parallel to the surface is enhanced.³⁰ For both CuBDC and CuCDC, the average dihedral angle between the (100) plane and the crystallographic plane defined by the carboxylate groups is 70° (ESI Figure S14 and Table S8[†]). Since

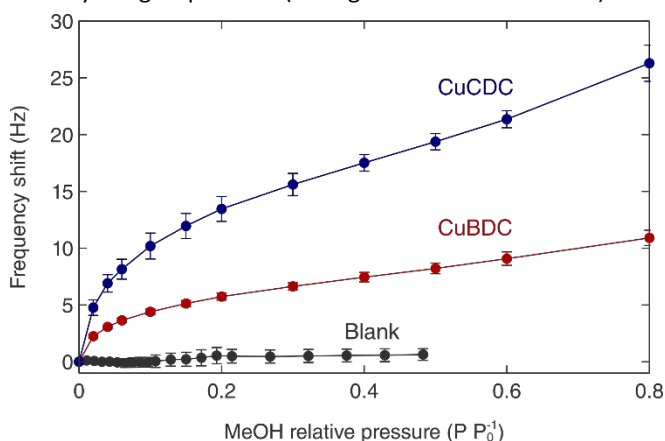


Figure 6 Gravimetric methanol uptake in CuCDC and CuBDC films. Resonance frequency shift of QCM crystals coated with CuCDC (blue) and CuBDC (red) films and an uncoated reference (black) as a function of relative pressure. Error bars correspond to the 95% confidence interval based on at least 7 measurements.

this angle is close to 90° , the observed difference in absorbance is explained by the (100) plane oriented parallel to the substrate and the resulting near-perpendicular orientation of the Cu-carboxylate bonds. The ratio of the symmetric and asymmetric carboxylate absorbance signals indicates a higher degree of orientation for CuCDC grown in a dry *versus* a humid atmosphere (8.7 and 6.2, respectively) and a higher degree of orientation for CuCDC than CuBDC (8.7 and 6.7, respectively) (ESI Table S7[†]).

Both CuBDC and CuCDC have one-dimensional pores parallel to the crystallographic *a*-axis. Therefore, (100)-oriented films of these materials have pores oriented perpendicular to the surface, thus ideally accessible for guest molecules (**Figure 4**). Conversely, CuBDC films prepared by liquid-phase epitaxy display a (001) orientation with pores oriented parallel to the substrate (ESI Figure S15[†]).³¹ To evaluate their porosity, CuCDC and CuBDC films were deposited by CVD on quartz crystal microbalance (QCM) crystals and the resonance frequency change was measured upon exposure to increasing methanol vapour concentrations. Both films take up significantly more methanol compared to a bare reference crystal, thus demonstrating the pore accessibility (**Figure 6**).

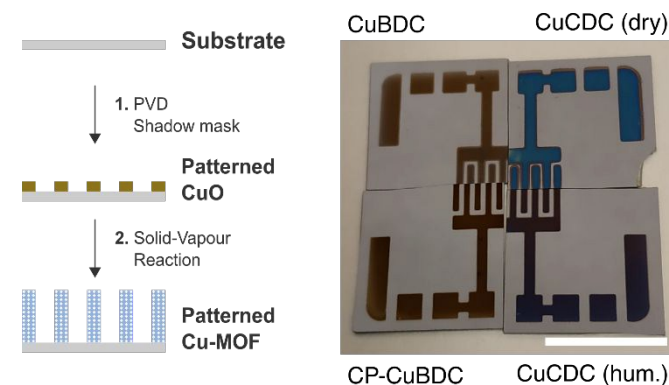


Figure 5 Patterned Cu-based MOF thin films. Left: schematic representation of the patterning sequence based on shadow mask CuO deposition. Right: patterned Cu-based MOF thin films. Scale bar = 1 cm.

The development of MOF-CVD methods will facilitate the integration of MOFs in microelectronics. While Stassen *et al.* demonstrated lift-off patterning for ZIF-8 MOF-CVD, we show the direct conversion of patterned CuO deposited by PVD through a shadow mask to patterned MOF films (Figure 5).¹⁸

In conclusion, we expanded MOF-CVD to thin films of copper dicarboxylate MOFs. To the best of our knowledge, these are the first crystalline and oriented porous materials deposited entirely from the vapour phase. Future MOF-CVD research will target even more porous Cu-based MOFs, such as the well-known HKUST-1 based on Cu(II) paddlewheels linked by 1,3,5-benzenetricarboxylate.³²

T.S. and I.S. thank the Research Foundation Flanders (FWO) for a SB-PhD fellowship and postdoctoral fellowship (1S53316N and 12L5417N). R.A. and P.F. acknowledge the funding from the European Research Council (ERC) under the European Union's Horizon 2020 research and innovation programme (grant agreements n° 716472 and 771834, acronyms: VAPORE and POPCRYSTAL), and the Research Foundation Flanders (FWO) for funding in the projects G083016N, 1529618N and 1501618N. This study is a result from the lead project Porous Materials @ Work (Graz University of Technology, Austria). We acknowledge the European Synchrotron Radiation Facility for provision of synchrotron radiation facilities and we would like to thank Oleg Konovalov and Andrey Chumakov for assistance in using beamline ID10. The authors are grateful to Steven De Feyter for access to AFM instrumentation and to Max L. Tietze for XPS data processing.

Conflicts of interest

There are no conflicts to declare.

Notes and references

- † Crystal structure codes from the CSD: CuCDC (SIWGUB), CuBDC (ZUBKEO), CP-CuBDC (KAKSUL). Calculated pore diameters obtained by Monte Carlo sampling using Zeo++.³³ Film expansion factor calculated from MOF/CP crystallographic density and experimental CuO density.
- 1 A. Corma, H. García and F. X. Llabrés i Xamena, *Chem. Rev.*, 2010, **110**, 4606–4655.
- 2 J.-R. Li, R. J. Kuppler and H.-C. Zhou, *Chem. Soc. Rev.*, 2009, **38**, 1477–1504.
- 3 I. M. Hönigke, I. Senkovska, V. Bon, I. A. Baburin, N. Bönisch, S. Raschke, J. D. Evans and S. Kaskel, *Angew. Chem. Int. Ed.*, 2018, **57**, 13780–13783.
- 4 I. Stassen, N. Burtch, A. Talin, P. Falcaro, M. Allendorf and R. Ameloot, *Chem. Soc. Rev.*, 2017, **46**, 3185–3241.
- 5 L. E. Kreno, K. Leong, O. K. Farha, M. Allendorf, R. P. Van Duyne and J. T. Hupp, *Chem. Rev.*, 2012, **112**, 1105–1125.
- 6 V. Stavila, A. A. Talin and M. D. Allendorf, *Chem. Soc. Rev.*, 2014, **43**, 5994–6010.
- 7 I. Stassen, D. De Vos and R. Ameloot, *Chem. – Eur. J.*, 2016, **22**, 14452–14460.
- 8 I. Stassen, N. Campagnol, J. Fransaer, P. Vereecken, D. D. Vos and R. Ameloot, *CrystEngComm*, 2013, **15**, 9308–9311.
- 9 J.-B. Lin, R.-B. Lin, X.-N. Cheng, J.-P. Zhang and X.-M. Chen, *Chem. Commun.*, 2011, **47**, 9185–9187. DOI: 10.1039/C9CC05161A
- 10 K. Uzarevic, T. C. Wang, S.-Y. Moon, A. M. Fidelli, J. T. Hupp, O. K. Farha and T. Friščić, *Chem Commun*, 2015, **52**, 2133–2136.
- 11 A. Pichon, A. Lazuen-Garay and S. L. James, *CrystEngComm*, 2006, **8**, 211.
- 12 S. Tanaka, K. Kida, T. Nagaoka, T. Ota and Y. Miyake, *Chem. Commun.*, 2013, **49**, 7884–7886.
- 13 K. Imawaka, M. Sugita, T. Takewaki and S. Tanaka, *Polyhedron*, 2019, **158**, 290–295.
- 14 X. Feng, C. Jia, J. Wang, X. Cao, P. Tang and W. Yuan, *Green Chem.*, 2015, **17**, 3740–3745.
- 15 C. Mottillo, Y. Lu, M.-H. Pham, M. J. Cliffe, T.-O. Do and T. Friščić, *Green Chem.*, 2013, **15**, 2121–2131.
- 16 United States, US8466285B2, 2013.
- 17 E. Virmani, J. M. Rotter, A. Mähringer, T. von Zons, A. Godt, T. Bein, S. Wuttke and D. D. Medina, *J. Am. Chem. Soc.*, 2018, **140**, 4812–4819.
- 18 I. Stassen, M. Styles, G. Greci, H. V. Gorp, W. Vanderlinden, S. D. Feyter, P. Falcaro, D. D. Vos, P. Vereecken and R. Ameloot, *Nat. Mater.*, 2016, **15**, 304–310.
- 19 L. D. Salmi, M. J. Heikkilä, E. Puukilainen, T. Sajavaara, D. Grosso and M. Ritala, *Microporous Mesoporous Mater.*, 2013, **182**, 147–154.
- 20 E. Ahvenniemi and M. Karppinen, *Chem. Commun.*, 2016, **52**, 1139–1142.
- 21 K. B. Lausund and O. Nilsen, *Nat. Commun.*, 2016, **7**, 13578.
- 22 H. Kumagai, M. Akita-Tanaka, K. Inoue, K. Takahashi, H. Kobayashi, S. Vilminot and M. Kurmoo, *Inorg. Chem.*, 2007, **46**, 5949–5956.
- 23 C. G. Carson, G. Brunnello, S. G. Lee, S. S. Jang, R. A. Gerhardt and R. Tannenbaum, *Eur. J. Inorg. Chem.*, 2014, **2014**, 2140–2145.
- 24 I. Platzman, R. Brener, H. Haick and R. Tannenbaum, *J. Phys. Chem. C*, 2008, **112**, 1101–1108.
- 25 T. Loiseau, C. Serre, C. Huguenard, G. Fink, F. Taulelle, M. Henry, T. Bataille and G. Férey, *Chem. – Eur. J.*, 2004, **10**, 1373–1382.
- 26 T. Stassin, S. Waitschat, N. Heidenreich, H. Reinsch, F. Puschke, D. Kravchenko, I. Stassen, J. van Dinter, R. Verbeke, M. Dickmann, W. Egger, I. Vankelecom, D. De Vos, R. Ameloot and N. Stock, *ChemRxiv*, DOI:10.26434/chemrxiv.8311235.v1.
- 27 K. Barthelet, J. Marrot, D. Riou and G. Férey, *Angew. Chem. Int. Ed.*, 2002, **41**, 281–284.
- 28 B. Schrodde, S. Pachmajer, M. Dohr, C. Röthel, J. Domke, T. Fritz, R. Resel and O. Werzer, *J. Appl. Crystallogr.*, 2019, **52**, 683–689.
- 29 S. Abdelouhab, M. François, E. Elkaim and P. Rabu, *Solid State Sci.*, 2005, **7**, 227–232.
- 30 V. P. Tolstoy, I. V. Chernyshova and V. A. Skryshevsky, *Handbook of Infrared Spectroscopy of Ultrathin Films: Tolstoy/Infrared Spectroscopy*, John Wiley & Sons, Inc., Hoboken, NJ, USA, 2003.
- 31 J. Liu, B. Lukose, O. Shekhah, H. K. Arslan, P. Weidler, H. Gliemann, S. Bräse, S. Grosjean, A. Godt, X. Feng, K. Müllen, I.-B. Magdau, T. Heine and C. Wöll, *Sci. Rep.*, 2012, **2**, 921.
- 32 S. S.-Y. Chui, S. M.-F. Lo, J. P. H. Charmant, A. G. Orpen and I. D. Williams, *Science*, 1999, **283**, 1148–1150.
- 33 T. F. Willems, C. H. Rycroft, M. Kazi, J. C. Meza and M. Haranczyk, *Microporous Mesoporous Mater.*, 2012, **149**, 134–141.